 doi:10.20944/preprints202210.0475.v1

Article

SCAND1 Reverts EMT and Suppresses Tumor Growth and Collective Migration

Takanori Eguchi [1,*], Eva Csizmadia [2], Thomas L. Prince [3], Barbara Wegiel [2] and Stuart K. Calderwood [4,*]

[1] Department of Dental Pharmacology, Graduate School of Medicine, Dentistry and Pharmaceutical Sciences, Okayama University, Okayama 700-8525, Japan; eguchi@okayama-u.ac.jp
[2] Department of Surgery, Division of Surgical Sciences, Cancer Research Institute, Beth Israel Deaconess Medical Center, Harvard Medical School, Boston, MA 02115, USA; ecsizmad@bidmc.harvard.edu; bwegiel@bidmc.harvard.edu
[3] Ranok Therapeutics, Waltham, MA 02451, USA; thomas.l.prince@gmail.com
[4] Department of Radiation Oncology, Beth Israel Deaconess Medical Center, Harvard Medical School, Boston, MA 02115, USA; scalderw@bidmc.harvard.edu
* Correspondence: eguchi@okayama-u.ac.jp (T.E.); Phone: +81 86 235 6661, Fax +81 86 235 6664, scalderw@bidmc.harvard.edu (S.K.C.); Phone: +1 617 667 4240, Fax: 617 667 4245,

Abstract: Epithelial-mesenchymal transition (EMT) is a reversible cellular program that transiently places epithelial (E) cells into pseudo-mesenchymal (M) cell states. The malignant progression and resistance of many types of carcinomas depends on EMT activation, partial EMT and hybrid E/M status in neoplastic cells. EMT is activated by tumor microenvironmental TGFβ signal and EMT-inducing transcription factors, such as ZEB1/2 in tumor cells. However, reverse EMT factors are less studied. We demonstrate that transcription factor SCAND1 can revert mesenchymal and hybrid E/M phenotype of cancer cells to a more epithelial, less invasive status and inhibit their proliferation and migration. SCAND1 is a SCAN domain-containing protein and hetero-oligomerizes with SCAN-zinc finger transcription factors, such as MZF1, for accessing DNA and transcriptional co-repression of target genes. We found that SCAND1-MZF1 co-expression and interaction correlated with maintaining epithelial features, whereas the simultaneous loss of SCAND1 and MZF1 correlated with mesenchymal features of tumor cells. Overexpression of SCAND1 over endogenous MZF1 in DU-145 prostate cancer cells reverted their hybrid E/M status into cobblestone morphology with increased epithelial adhesion by E-cadherin and β-catenin relocation. Consistently, co-expression analysis in TCGA PanCancer Atlas revealed that both SCAND1 and MZF1 co-express and are negatively correlated with EMT driver genes, including CTNNB1, ZEB1, ZEB2 and TGFBR, in prostate tumor specimens. In addition, SCAND1 overexpression suppressed tumor cell proliferation by reducing the MAP3K-MEK-ERK signaling pathway. Of note, SCAND1-overexpressing DU-145 cells migrated slower than control cells with decreased lymph node metastasis of prostate cancer in a mouse tumor xenograft model. Kaplan-Meyer analysis showed high expression of MZF1 and SCAND1 to correlate with better prognoses in pancreatic cancer and head and neck cancers, although with poorer prognosis in kidney cancer. Overall, these data suggest that the combination of SCAND1-MZF1 complexes may revert the EMT mechanism in cancer to establish an epithelial phenotype. These effects seem to include co-repression of EMT-driver genes and suppression of tumor cell proliferation via inhibition of the MAP3K-MEK-ERK signaling pathway.

Keywords: epithelial-to-mesenchymal transition (EMT); hybrid EMT; partial EMT; mesenchymal-to-epithelial transition (MET); SCAND1; SCAN zinc finger; MZF1; cancer prognosis

1. Introduction

Epithelial–mesenchymal transition (EMT) is a reversible cellular program that transiently transforms epithelial cells into pseudo-mesenchymal cell states [1-6]. During this process, epithelial cells progressively lose their cobblestone appearance observed in monolayer cultures to adopt a spindle-shaped, mesenchymal morphology. EMT plays

 doi:10.20944/preprints202210.0475.v1

significant roles in the malignant progression of many types of carcinoma [7-10]. During the tumor progression, the EMT program confers multiple traits associated with high-grade malignancy on carcinoma cells [7,11,12]. Normally, the cells forming epithelial sheets in adult various tissues display apical–basal polarity and are held together laterally by adherens junctions and tight junctions. Adherens junctions are formed by cell surface epithelial cadherin (E-cadherin) molecules encoded by ECAD gene, while tight junctions are formed by tight junction proteins TJP (also known as *zonula occludens*: ZO) and epithelial cell adhesion molecule EpCAM (also known as CD326) [10,13]. This organization is essential for the structural integrity of epithelia. Upon activation of EMT, E-cadherin expression is repressed, which leads to the loss of the typical polygonal, cobblestone morphology of epithelial cells [10,12]. Cells acquire a spindle-shaped mesenchymal morphology and express markers including vimentin (encoded by VIM gene), neural cadherin (N-cadherin) and fibronectin [3]. Besides, recent studies have shown that EMT is rarely fully executed in tumor cells, while the process is rather gradual and often remains incomplete, termed partial EMT, hybrid EMT or hybrid E/M [2,14]. Hybrid EMT was identified by co-expression of epithelial (EpCAM+) and mesenchymal (Vim+) marker genes in an autochthonous murine prostate cancer model [15]. Consistently, hybrid EMT of prostate cancer cells within a tumor organoid (tumoroid) was identified by co-expression of epithelial (E-cadherin+ EpCAM+) and mesenchymal (Vimentin+) markers with enhanced stemness [13]. Another group identified different tumor transition states occurring during EMT in cancer progression and introduced the term hybrid EMT [16,17]. Dynamic induction of EMT and MET changes cellular phenotypes of carcinoma cells. Drug sensitivity, proliferation, and response to apoptosis signals are highest in more epithelial states, whereas drug efflux, invasion, and immuneevasion are highest in more mesenchymal states [18,19]. A hybrid EMT state provides maximal stemness, tumor initiation capacity, and ability to adapt to environmental changes [18].

The process of EMT is orchestrated by EMT-inducing transcription factors (EMT-TFs), which act combinatorially to induce expression of genes that promote the mesenchymal cell state and repress the expression of genes that maintain the epithelial state [1-4,6]. These include the zinc-finger E-box binding homeobox factors ZEB1 and ZEB2, SNAIL (also known as SNAI1), SLUG (also known as SNAI2) and the basic helix–loop–helix factors TWIST1 and TWIST2. These EMT-TFs regulate the expression of each other, and in different combinations induce the expression of hundreds of genes associated with the mesenchymal state (Vimentin, N-cadherin, fibronectin, β1 and β3 integrins, and metalloproteinases) while repressing genes associated with the epithelial state (E-cadherin, EpCAM, occludins, claudins, and cytokeratins). However, less is known about anti-EMT transcription factors (TF) that reverse EMT programs and place pseudo-mesenchymal cancer cells back into an epithelial phenotype. Here we aim to address such factors.

The SREZBP-CTfin51-AW1-Number 18 cDNA (SCAN) domain is a leucine-rich oligomerization domain, highly conserved among the SCAN domain-containing transcription factor (SCAN-TF) family. This family contains more than 50 family members, most of which contain a zinc finger (ZF) domain: hence SCAN-ZF factors [20-24]. Myeloid zinc finger 1 (MZF1), also known as ZSCAN6 or ZNF42 belongs to the SCAN-ZF family and contains an N-terminal SCAN domain, a linker region, and a C-terminal DNA binding domain [25-27]. Many studies have identified MZF1 as an oncogenic transcription factor [25,28-31] and cancer stemness factor [32,33]. However, MZF1 can also function as a tumor suppressor that, for instance represses MMP2 in cervical cancer [34] and mediates oncogene-induce senescence [35]. Furthermore, MZF1 is also important in a protumorigenic microenvironment by activating osteopontin gene in mesenchymal stem cells, leading to transformation into cancer-associated fibroblasts (CAF) [36] and VEGF gene in tumor endothelial cells [37].

While there are more than 50 types of SCAN-TFs, a few zinc fingerless SCAN domain-only proteins also exist [21,22]. SCAND1 is such a SCAN domain-only protein and hetero-oligomerizes with other SCAN-ZFs, including MZF1, through inter-SCAN domain interactions to repress transcription [23,24,28,38]. Hetero-oligomerization between SCAN

Preprints (www.preprints.org) | NOT PEER-REVIEWED | Posted: 31 October 2022 doi:10.20944/preprints202210.0475.v1

domain-only molecules and SCAN-ZF molecules transform their roles, leading to formation of a transcriptional repressor complex [23,24,28,38]. Indeed, SCAND1 represses the *CDC37* gene (encoding cell division control 37) by interacting with MZF1 and suppressing prostate cancer progression [28]. However, the potential involvement of SCAND1-MZF1 in EMT has not been addressed. Here, we investigate the involvement of SCAND1-MZF1 in reverting EMT in cancer.

2. Materials and Methods

2.1. Cell culture

Prostate cancer cell lines PD-145 and PC-3 were provided by ATCC and cultured in DMEM and RPMI medium, respectively, with 10% FBS. The prostate normal epithelial cell line immortalized with SV40 large T antigen (PNT2) was purchased from Sigma and cultured in RPMI medium with 10% FBS. Human normal prostate epithelial cells (PrEC) were purchased from Lonza (Basel, Switzerland) and cultured in prostate epithelial cell basal medium supplemented with bovine pituitary extract, hydrocortisone, hEGF, epinephrine, transferrin, insulin, retinoic acid, triiodothyronine and GA-1000 (Lonza).

2.2. qRT-PCR

qRT-PCR was performed as previously described [39,40]. Total RNA was prepared with DNase I treatment using RNeasy (Qiagen, Hilden, Germany). cDNA was synthesized using QuantiTect kit (Qiagen), a mixture of oligo dT and random primers, then diluted 5 fold in 10 mM Tris-Cl and 0.1 mM EDTA buffer. A step dilution of the cDNA pool was prepared as a standard for relative expression. cDNA (4–10 µl), 0.25 µM of each primer and 10 µl SYBR green 2x Master Mix (Applied Biosystems, Waltham, MA) were mixed and filled up to a 20 µl of a reaction mixture. We designed and used primer pairs: h ECAD 1937F, 5'-agg aat cca aag cct cag gt-3'; h ECAD 2065R, 5'-ttg ggt tgg gtc gtt gta ct -3'; h VIM 892F, 5'-agg tgg acc agc taa cca ac -3'; h VIM 1010R, 5'-ggc ttc ctc tct ctg aag ca -3'; h 18s rRNA 1245F, 5'-gac tca aca cgg gaa acc tc-3'; h 18s rRNA 1364R, 5'-aga caa atc gct cca cca ac-3'. Initial denaturation was performed at 95°C 10 min, and 40 cycles of PCR were run at 95°C for 15 sec and at 60°C for 1 min. Single amplicons were confirmed by dissociation curve analysis. Relative mRNA expression levels were obtained as compared with the standard described above.

2.3. cDNA transfection and stable cell cloning

We used pcDNA3/MZF1^{Flag} and pCMV6/SCAND1$^{myc\text{-}Flag}$ (variant 1, purchased from OriGene, accession number NM_016558) as previously described [28]. DU-145 cells were transfected with these plasmids and pcDNA3 vector using Lipofectamine 2000 (Thermo Fisher Scientific) and cultured with 0.4, 0.8 and 1.6 µg/ml of geneticin for 2 weeks to establish clone 1 (c1), clone 2 (c2) and clone 3 (c3), respectively. The survived cells were used for subsequent assays.

2.4. Lentiviral infection and cell cloning

Lentivirus infection was performed as previously described [12]. A lentiviral expression vector for SCAND1^{HA3} was constructed from pCMV6/SCAND1$^{myc\text{-}Flag}$ [28] and pcDNA3.1-HA3 that contains triple hemagglutinin (HA) tag [40] via gene recombination. The pLV-SCAND1^{HA3} (4 µg), psPAX2 (3 µg) and pVSV-G (1 µg) were cotransfected using Lipofectamine LTX and Plus reagents (Thermo Fisher Scientific) into HEK293FT cells cultured in DMEM supplemented with 10% heat-inactivated (HI) FBS, penicillin and streptomycin. After 10 hours, the medium was replaced with a fresh one. After 48 hours, cell culture supernatant was collected and centrifuged at 500 x g for 10 min. The supernatant was filtered through Millex-HP 0.45-µm polyethersulfone low protein-binding filters (Millipore, Billerica, MA). DU-145 cells were cultured in the half-and-half mixture of the conditioned medium containing pseudo-virus particles and DMEM with 10% FBS supplemented with 5 µg/ml of polybrene and centrifuged for spinfection at 800 x g for 1 hour

Preprints (www.preprints.org) | NOT PEER-REVIEWED | Posted: 31 October 2022 doi:10.20944/preprints202210.0475.v1

at room temperature (RT). Cells were cultured in DMEM with 10% HI-FBS and 1 μg/ml of puromycin for 10 days. The survived cells were used for subsequent assays.

2.5. Western Blotting

Protein sampling, SDS-PAGE and western blotting were performed as previously described [13,28,40]. Cells cultured in 60-mm dishes were washed with ice-cold PBS. Cells were soaked in 500 μl of ice-cold CelLytic M (Sigma, St. Louis, MO) supplemented with a cocktail of protease inhibitors and phosphatase inhibitors (Thermo Fisher Scientific) and incubated for 15 min on a shaker. Cells were scraped from the bottom of the dish and collected into 1.5-ml tubes. The lysate was centrifuged at 12,000 x g for 15 min, and the supernatant was collected as cell lysate. The pellet was stored as an insoluble fraction. The protein concentration was measured using BCA protein assay kit (Thermo Fisher Scientific). The equal amounts of protein samples (10–30 μg) were mixed with 4 x Laemmli sample buffer, boiled for 5 min at 95°C, and then loaded to 12% polyacrylamide gels for SDS-PAGE. Proteins were transferred to PVDF membranes. Membranes were soaked in a blocking buffer containing 5% skim milk in TBS-T for 1 hour, incubated with primary antibodies in the blocking buffer at 4°C overnight, and then incubated with secondary antibodies in the blocking buffer at RT for 1 hour. Membranes were washed thrice with TBS-T for 10 min at RT between the steps. Proteins were detected by chemiluminescence reactions. We used antibodies against SCAND1 (ab64828, Abcam, Cambridge, UK), MZF1 (C10502, Assay Biotechnology, Fremont, CA), Flag-tag (M2, Sigma), and Vimentin (V9, MA1-06909, Thermo Fisher Scientific). Antibodies against E-cadherin (#4065), ZO-1 (#5406), phosphorylated ERK-1/2 Thr202/Thr204 (D13.14.4E, #4370P), total ERK-1/2 (137F5, #4695), phosphorylated NF-κB p65 S536 (93H1, #3033S), total NF-κB p65 (#4674S) and HSP90β (#5087) were purchased from Cell Signaling Technologies (CST, Danvers, MA).

2.6. Immunocytochemistry and CLSM

Immunocytochemistry and confocal laser scanning microscopy (CLSM) were performed as previously described [40,41]. Cells were cultured on 120-mm round coverslips coated with poly-D-Lysine/Laminin coat (BD Bioscience, Franklin Lakes, NJ) in 4-well plates (Thermo Fisher Scientific). Cells were fixed with 4% paraformaldehyde for 10 min and washed with PBS twice. Cells were permeabilized with 0.1% Triton X-100 for 10 min and washed with PBS twice. Cells were incubated in a blocking buffer containing 3% normal goat serum in PBS for 30 min, with primary antibodies at 4°C overnight and then secondary antibodies at RT for 1 hour in the blocking buffer. Cells were washed three times with PBS for 5 min between the steps. Cells were mounted within ProLong Gold Antifade Mountant (Thermo Fisher Scientific). Fluorescence images were acquired using Axio Vision CLSM (Zeiss, Oberkochen, Germany) with a camera AxioCam MR3 (Zeiss) and a filter set for DAPI, GFP, Cy3.5 (excitation wavelength: 580 nm) and Cy5 (excitation wavelength: 650 nm). We used combinations of anti-mouse (Ms) IgG and anti-rabbit (Rb) IgG against: HA-tag (16B12, Covance, Ms, 1:1000) and MZF1 (C10502, Assay Biotechnology, Rb, 1:50); β-catenin (15B8, ab6301, Abcam, Ms) and E-cadherin (24E10, #4065, CST, Rb, 1:200). Anti-mouse and anti-rabbit IgG conjugated with Alexa Fluor 488 or 594 (Thermo Fisher Scientific, 1:1000) were used as secondary antibodies.

2.7. Xenograft

One million cells were subcutaneously injected to the flanks of nude mice (Charles River, Wilmington, MA). After 2 months, mice were sacrificed, and tumors and pelvic lymph nodes were harvested. All surgeries were performed under isoflurane anesthesia, and efforts were made to minimize mice suffering. All the animals were housed under specific pathogen-free conditions.

 doi:10.20944/preprints202210.0475.v1

2.8. Immunohistochemistry (IHC)

Tissues were fixed in formalin for 48 h, dehydrated in a series of alcohol solutions with increasing percentages, treated with xylene, and then embedded in paraffin. Paraffin blocks were cut into 5 μm sections using a microtome and mounted on microscope glass slides. Sections were deparaffinized and rehydrated. Antigens were retrieved with 0.1 M sodium citrate pH 6.0 in a high-pressure cooker. For immunofluorescence, sections were incubated within 10% normal serum for 15 min, primary antibodies against SCAND1 (ab64828, Abcam, Rb) and E-cadherin (#14472, CST, Ms) overnight at 4°C, secondary antibodies against rabbit IgG conjugated with Alexa Fluor 594 and mouse IgG conjugated with Alexa Fluor 488 at RT for 1 hour, and Hoechst. Slides were washed three times with PBS between staining steps. Fluorescence images were acquired using Axio Vision CLSM (Zeiss). Alternatively, sections were incubated with primary antibodies against Vimentin (V9, MA1-06909, Thermo Fisher Scientific) or Ki-67 (DAKO) overnight at 4°C followed by biotinylated secondary antibodies (Vector Laboratories, Newark, CA) at RT for 1 hour. Slides were washed twice for 5 min in PBS between the staining steps. Sections were incubated with avidin-biotin peroxidase complexes of the ABC kit (Vectastain, Vector Laboratories) at RT for 30 min and with 3, 3′-Diaminobenzidine (ImmPACT™ DAB HRP Substrate, Vector Laboratories). Nuclei were counterstained with hematoxylin. Sections were covered with mounting medium and coverslips, then evaluated microscopically (Nikon, Minato City, Tokyo).

2.9. Coexpression analysis

Coexpression was analyzed using cBioPortal as previously described [12,28,41]. A data set of prostate adenocarcinomas (TCGA, PanCancer Atlas; 494 patients/samples) were analyzed with Spearman's rank correlation coefficient of coexpression. The coexpression of SCAND1 and MZF1 was first examined. Then, coexpression of SCAND1 and MZF1 versus genes encoding mitogen-activated protein kinases (including MAP3Ks, MAP2Ks and MAPKs), TGFβ receptors (TGFBR1, TGFBR2 and TGFBR3), EMT-TFs (including ZEB1 and ZEB2) and β-catenin (CTNNB1) were analyzed. Genes of which Spearman's correlation versus both MZF1 and SCAND1 expression was less than –0.3 were depicted in graphs and listed in a table with p- and q-values.

2.10. Kaplan-Meyer analysis

Kaplan-Meier plotting from RNA-seq data was performed using KM plotter and GEPIA 2 [42,43]. We analyzed the overall survival of patients suffering from pancreatic ductal adenocarcinoma (DAC) n=177, kidney renal clear cell carcinoma (RCC) n=530, head and neck squamous cell carcinoma (SCC) stage III (n=78) using KM plotter with auto select best cutoff, and prostate adenocarcinoma (AC) n=639 using GEPIA 2.

2.11. Statistics

Values of two groups were compared with an unpaired Student's *t*-test. $P < 0.05$ was considered to indicate statistical significance. Data were expressed as Mean ± SD unless otherwise specified.

3. Results

3.1. SCAND1 and MZF1 co-expression correlated with epithelial phenotype of tumor cells

Prostate cancer cell line PC-3 is the most malignant, metastatic cell line employed here, while DU-145 is a moderately metastatic, prostate adenocarcinoma cell line [13,28,44]. We also used prostate normal epithelial cell line PNT2 and first examined the morphologies of PC-3, DU-145 and PNT2 in the monolayer culture. Most of the PC-3 cell population exhibited a spindle-shaped, mesenchymal morphology in culture, while DU-145 cells were a mixed population of spindle-shaped, mesenchymal cells and the remainder with the cobblestone morphology, a characteristic of epithelial cells, indicating that

 doi:10.20944/preprints202210.0475.v1

DU-145 was a hybrid E/M status (Figure 1A). In contrast, PNT2 cell populations contained only epithelial cells with the cobblestone morphology.

To confirm the link between morphology and gene expression, we next examined differential gene expression of ECAD and VIM among these cell types. ECAD mRNA was highly expressed in normal prostate epithelial cells and PNT2 cells, while being reduced in DU-145 and undetectable in PC-3 cells (Figure 1B), consistent with their morphology. VIM mRNA was highly expressed in PC-3 and DU-145 but lost in PNT2 cells (Figure 1C), again consistent with their morphology.

To assess the involvement role of SCAND1 and MZF1 in the E/M status, we performed western blotting of MZF1, SCAND1, and epithelial and mesenchymal markers. SCAND1 and MZF1 were well expressed in epithelial cell line PNT2 and normal prostate cells, although reduced in DU-145 and at minimal levels in PC-3 cells (Figure 1D). E-cadherin and Vimentin levels were consistent with their mRNA expression. ZO-1 (also known as tight junction protein 1: TJP1) was detected in epithelial cell line PNT2 and normal prostate cells, at reduced levels in DU-145 and not detected in PC-3 cells. These data suggested that SCAND1 and MZF1 expression correlates with epithelial features, whereas the loss of SCAND1 and MZF1 is correlated with mesenchymal features.

Next, we examined whether SCAND1 and MZF1 expression levels were correlated in clinical prostate adenocarcinoma specimens. Indeed, SCAND1 and MZF1 expression was significantly correlated in prostate adenocarcinomas, indicating that these SCAN domain proteins are consistently co-expressed (Figure 1E).

To confirm intracellular SCAND1-MZF1 interaction, we next examined the subcellular localizations of the two factors by immunostaining and CLSM. The overexpressed $SCAND1_{HA3}$ and endogenous MZF1 were well colocalized in the nuclei of DU-145 cells, suggesting that SCAND1 and MZF1 could directly interact each other (Figure 1F).

These data suggested that SCAND1-MZF1 co-expression and interaction is involved in maintaining epithelial features, whereas the simultaneous loss of SCAND1 and MZF1 correlated with a mesenchymal and E/M phenotypes in tumor cells.

Preprints (www.preprints.org) | NOT PEER-REVIEWED | Posted: 31 October 2022 doi:10.20944/preprints202210.0475.v1

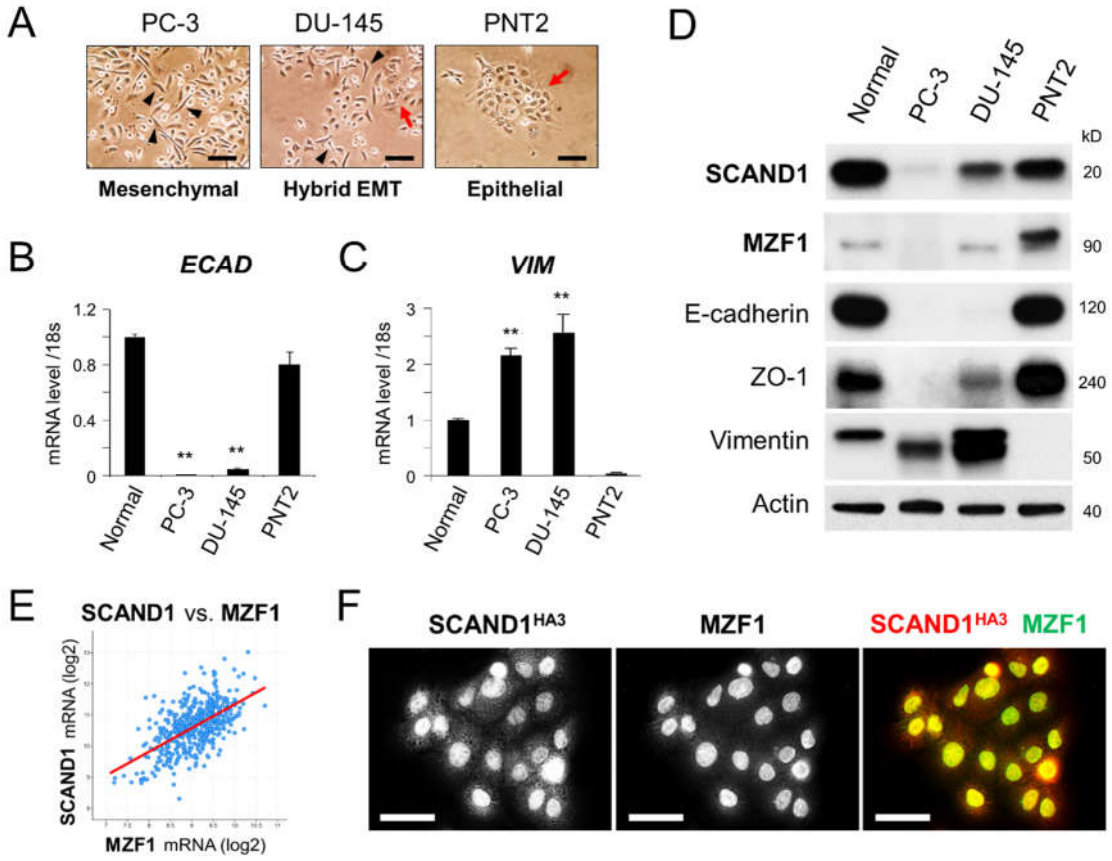

Figure 1. SCAND1 and MZF1 coexpression is involved in epithelial features of tumor cells. (A) Morphologies of PC-3, DU-145 and PNT2 cells. Arrowheads indicate spindle-shaped mesenchymal cells. Red arrows indicate polygonal, cobblestone-like epithelial cells. PC-3 is mesenchymal. DU-145 is hybrid EMT status. PNT2 is epithelial. Scale bars, 100 μm. (B, C) ECAD and VIM mRNA expression evaluated by qRT-PCR. **p<0.01 (versus Normal), n=3. Normal, normal prostate cells. (D) Western blotting of SCAND1, MZF1, E-cadherin, ZO-1 and Vimentin. Actin, loading control. Data of SCAND1 and actin were also published in ref [28]. (E) Coexpression analysis of SCAND1 and MZF1 mRNA in prostate adenocarcinoma specimens. (F) Colocalization of SCAND1 and MZF1 in nuclei. DU-145 cells were infected by lentivirus for expressing $SCAND1^{HA3}$. SCAND1 (red) and endogenous MZF1 (green) were immunostained and visualized using CLSM. Scale bars, 100 μm.

3.2. SCAND1 and MZF1 inhibit tumor cell proliferation and reverse EMT

To examine whether SCAND1 and MZF1 could alter tumor cell proliferation and EMT, we next overexpressed full-length $SCAND1^{Flag}$ and $MZF1^{Flag}$ using plasmid vectors (Figure 2A). In these experiments, we assume that the intracellular effects of SCAND1, which lacks a DNA-binding domain, are mediated by binding a SCAN-ZF partner, most likely MZF1 and forming a repressive heterodimer [25]. We also assume that MZF1 overexpression leads to increased formation of transcriptionally active MZF1 homodimers and titrates down level of endogenous MZF-SCAND1 heterodimers. Overexpression of $SCAND1^{Flag}$ and $MZF1^{Flag}$ were confirmed in COS7 cells (Figure 2B). We next transfected these plasmids into DU-145 cells and established stable clones that each overexpress $SCAND1^{Flag}$ and $MZF1^{Flag}$. Of note, overexpression of SCAND1 changed the DU-145 cells from the hybrid EMT status into a cobblestone-like epithelial morphology (Figure 2C). Both SCAND1 or MZF1 overexpression significantly inhibited tumor cell proliferation, while SCAND1 overexpression more significantly inhibited it (Figure 2D).

We next performed western blotting for E-cadherin, Vimentin, phosphorylated MAPK-ERK1/2 and NF-κB to confirm the role of SCAND1 and MZF1 in regulation of epithelial, mesenchymal, and cell proliferation markers. E-cadherin was markedly increased

 doi:10.20944/preprints202210.0475.v1

by SCAND1 overexpression and slightly by MZF1 overexpression (Figure 2E). Vimentin was markedly reduced by SCAND1 overexpression, although increased by MZF1 overexpression. These data suggested that SCAND1 reverses EMT in DU-145 cells and induces epithelial status. On the other hand, MZF1 overexpression enhanced hybrid EMT status by increasing both mesenchymal and epithelial markers.

Phosphorylated MAPK-ERK-1/2 levels were markedly reduced by SCAND1 overexpression, although not markedly affected by MZF1 overexpression (Figure 2E). In addition, phosphorylated NF-κB p65 (also known as RelA) was markedly reduced by SCAND1 overexpression, although not markedly altered by MZF1 overexpression. HSP90β, a constitutively expressed type of HSP90 often used as a loading control, was not markedly altered by the overexpression.

To verify whether the subcellular localization of β-catenin and E-cadherin were altered by SCAND1 and MZF1 overexpression, we next performed immunocytochemistry observed under CLSM. β-Catenin was accumulated in the nuclei of the non-transfected and MZF1-overexpressed DU-145 cells, while this versatile protein was also localized at intercellular adhesin sites in the hybrid EMT status (Figure 2F). In contrast, SCAND1 overexpression markedly reduced nuclear β-catenin and led to relocation to intercellular adhesion sites formed by E-cadherin. E-cadherin was faintly detectable in the cytoplasm and possibly in nuclei of non-transfected and MZF1-overexpressed cells. In contrast, SCAND1 overexpression markedly induced functional E-cadherin that formed epithelial intercellular adhesion.

These data suggested that SCAND1 reduces tumor cell proliferation by inhibiting the MEK-ERK signaling pathway, reverses EMT, and transduces prostate tumor cells into epithelial status.

Preprints (www.preprints.org) | NOT PEER-REVIEWED | Posted: 31 October 2022 doi:10.20944/preprints202210.0475.v1

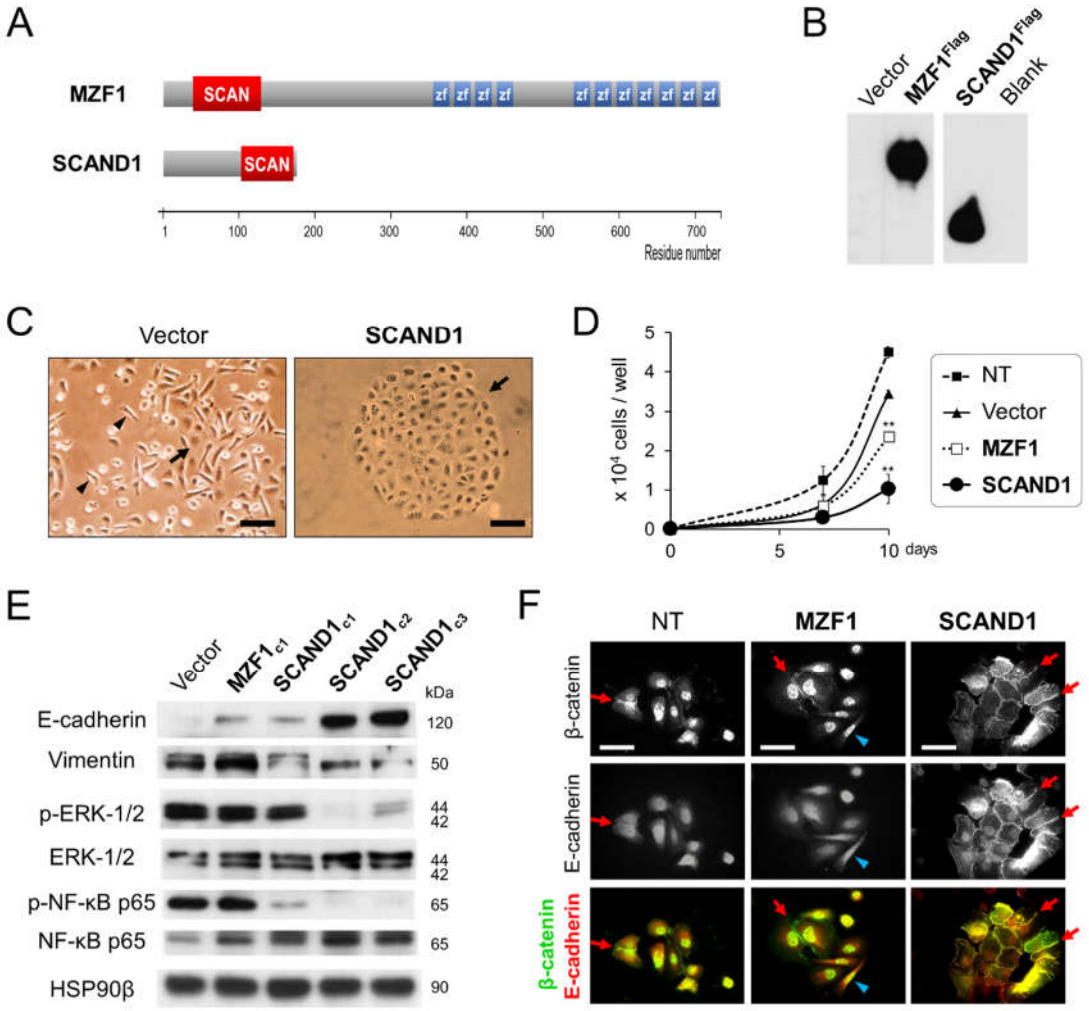

Figure 2. SCAND1 inhibits tumor cell proliferation and reverts EMT to establish epithelial adhesion. (A) Structures of MZF1 and SCAND1. zf, zinc finger motif. (B) Western blotting of $MZF1^{Flag}$ and $SCAND1^{Flag}$ expressed in COS7 cells. (C–F) Plasmid for overexpressing SCAND1 and MZF1 or the control pcDNA3 vector were transfected into DU-145, and stable cells were cloned. (C) Morphologies of SCAND1-overexpressed and control vector-transfected DU-145 cells. Arrowheads indicate spindle-shaped mesenchymal cells. Arrow indicates polygonal, cobblestone-like epithelial cells. Scale bars, 100 μm. (D) Cell proliferation curves. NT, non-transfected DU-145 cells. Vector, transfected with pcDNA3 vector. (E) Western blotting of E-cadherin, Vimentin, phosphorylated or total ERK-1/2 and NF-κB p65. HSP90β, loading control. (F) Subcellular localization of β-catenin and E-cadherin observed under CLSM. Red arrows indicate epithelial intercellular adhesion. Blue arrowheads indicate spindle-shaped mesenchymal cells. Scale bars, 100 μm.

3.3. SCAND1 and MZF1 expression negatively correlates with gene expression of MAP3Ks (MEKKs), MAPKs and EMT drivers

We have shown the coexpression and direct interaction of SCAND1 and MZF1 in Figure 1. To determine whether SCAND1-MZF1 could be involved in regulation of the gene expression of MAPKs and EMT drivers, we next investigated coexpression signatures of SCAND1 and MZF1 versus gene expression of MAPKs (including MAP3Ks) and EMT drivers, including CTNNB1 (encoding β-catenin), ZEB1 and ZEB2, and TGFBRs (encoding TGFβ receptors). Of note, we found that SCAND1 and MZF1 expression negatively correlated with expression of two MAP3K genes (MAP3K1(MEKK2) and MAP3K2(MEKK1)) and two MAPK genes (MAPK1(ERK2) and MAPK14(p38Alpha)) (Table 1, Figure 3A, 3B). These data suggested that SCAND1-MZF1 could mediate versatile repression of the MAP3Ks (MEKK1 and MEKK2) genes, which are essential for the phosphorylation of MAPKKs (MEK) and subsequent ERK.

Preprints (www.preprints.org) | NOT PEER-REVIEWED | Posted: 31 October 2022 doi:10.20944/preprints202210.0475.v1

Regarding EMT drivers, both SCAND1 and MZF1 expression negatively correlated with CTNNB1 expression in prostate tumor specimens (Figure 3C). Moreover, SCAND1 and MZF1 expression also negatively correlated with ZEB1 and ZEB2 expression (Figure 3D). These data suggested that SCAND1-MZF1 could repress ZEB1, ZEB2, and CTNNB1 genes, an effect that might reverse the EMT phenotype, consistent with the data from cell biology in Figure 2. Furthermore, SCAND1 and MZF1 co-expression was also negatively correlated with TGFBR1, TGFBR2 and TGFBR3 gene expression (Figure 3E), suggesting that SCAND1-MZF1 could reduce TGFβ receptors to narrow down TGFβ signals emanating from the microenvironment to tumor cells.

These data suggested that SCAND1-MZF1 could co-repress gene expression of MAP3Ks (MEKKs) and MAPKs to inhibit tumor cell proliferation; vise versa, loss of SCAND1-MZF1 could release gene expression of MEKKs and MAPKs to activate tumor cell proliferation. Moreover, SCAND1-MZF1 could co-repress gene expression of CTNNB1, ZEB1/2, and TGFBR1/2/3 to revert EMT; vise versa, loss of SCAND1-MZF1 could release gene expression of CTNNB1, ZEB1/2 and TGFBR1/2/3 to activate EMT.

Table 1. Correlated gene expression of SCAND1 and MZF1 versus MAP3K, MAPK, CTNNB1, ZEB, and TGFBR.

Correlated gene	SCAND1			MZF1			Alternative name
	Spearman's correlation	p-Value	q-Value	Spearman's correlation	p-Value	q-Value	
MAP3K2	-0.715	3.37E-78	3.32E-76	-0.382	1.40E-18	1.36E-17	MEKK2
MAP3K1	-0.617	5.63E-53	1.15E-51	-0.347	2.13E-15	1.53E-14	MEKK1
MAPK1	-0.633	1.40E-56	3.43E-55	-0.548	5.07E-40	2.47E-38	ERK2
MAPK14	-0.564	8.68E-43	1.08E-41	-0.457	8.33E-27	1.70E-25	p38Alpha
CTNNB1	-0.621	5.48E-54	1.18E-52	-0.517	4.68E-35	1.67E-33	–
ZEB2	-0.433	5.85E-24	3.24E-23	-0.381	1.72E-18	1.66E-17	–
ZEB1	-0.309	2.35E-12	7.43E-12	-0.353	7.00E-16	5.28E-15	–
TGFBR2	-0.373	9.33E-18	3.88E-17	-0.362	1.14E-16	9.26E-16	–
TGFBR3	-0.334	2.65E-14	9.24E-14	-0.384	9.96E-19	9.85E-18	–
TGFBR1	-0.301	8.14E-12	2.50E-11	-0.487	1.09E-30	2.95E-29	–

Preprints (www.preprints.org) | NOT PEER-REVIEWED | Posted: 31 October 2022 doi:10.20944/preprints202210.0475.v1

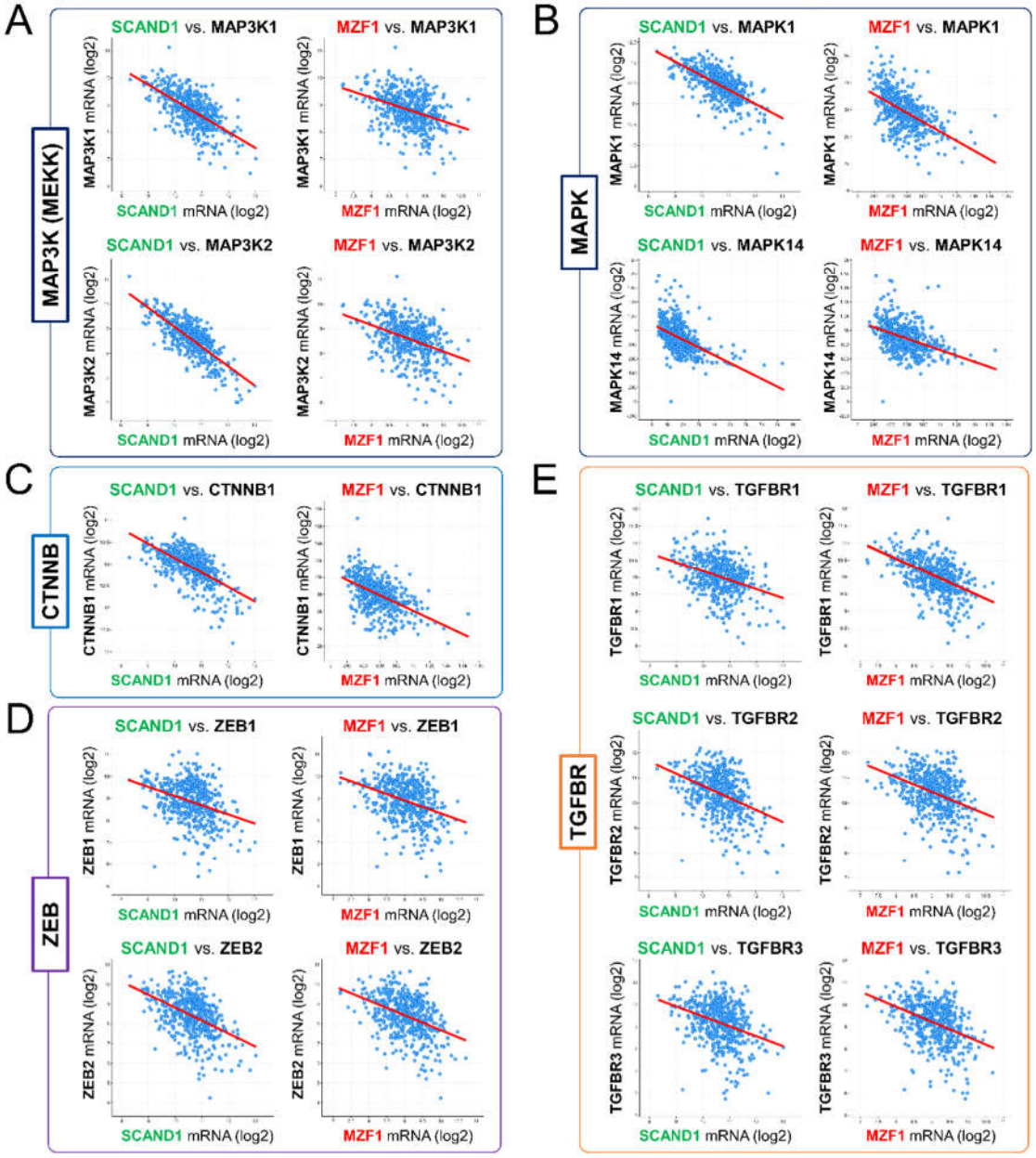

Figure 3. SCAND1 and MZF1 expression negatively correlated with gene expression of MAP3Ks (MEKKs), MAPKs, and EMT drivers in prostate tumors. Coexpression of SCAND1 and MZF1 were analyzed versus (A) MAP3K1 (MEKK1) and MAP3K2 (MEKK2), (B) MAPK1 (ERK2) and MAPK14 (p38Alpha), (C) CTNNB1 (encoding β-catenin), (D) ZEB1 and ZEB2, and (E) TGFβ receptors (TGFBR1, TGFBR2 and TGFBR3) in patients-derived prostate adenocarcinoma specimens.

3.4. SCAND1 overexpression inhibited collective migration and lymph-node metastasis of prostate cancer

Tumor cell migration and invasion are crucial processes in the initiation of metastasis, and hybrid EMT is known to be involved in these processes [18,45]. Metastatic prostate cancer often disseminate to pelvic lymph nodes [13,46]. Recent studies have shown that tumor budding of 5–20 cells collectively migrated and invaded stroma, a process known as collective migration [47,48]. We have recently shown that SCAND1 overexpression could inhibit tumor growth of prostate cancer cells in vivo [28]. We next used a mouse tumor xenograft model to examine whether SCAND1 could inhibit tumor cell EMT, migration, and metastasis. Colocalized expression of E-cadherin was seen in/around the cells overexpressing SCAND1, indicating that SCAND1 influenced the tumor cells towards an epithelial phenotype (Figure 4A). Vimentin was abundantly expressed in the control

Preprints (www.preprints.org) | NOT PEER-REVIEWED | Posted: 31 October 2022 doi:10.20944/preprints202210.0475.v1

tumors, although markedly reduced in the SCAND1-overexpressing cells (Figure 4B). These data suggested that SCAND1 reversed EMT in prostate tumor cells to a more epithelial status in vivo.

Ki-67, a marker of proliferating tumor cells, was suppressed by SCAND1 overexpression in in-vivo tumors (Figure 4C). Of note, collective migration of Ki67$^+$ tumor cells was seen budding from the tumor to invade stroma in the control tumors only but not in SCAND1-overexpressing tumors.

Next, we examined whether SCAND1 overexpression in prostate tumors could alter pelvic lymph node metastasis in the mouse xenograft model. Lymph node metastases were found in 100% (4/4) of the control mice, although reduced to 25% (1/4) in the SCAND1-overexpressing tumor xenograft mice (Figure 4D). The average rate of pelvic lymph node metastasis was 70% in the control mice versus 25% in the SCAND1-overexpressing tumor xenograft mice.

These data suggest that SCAND1 overexpression inhibited prostate cancer migration and lymph-node metastasis in vivo.

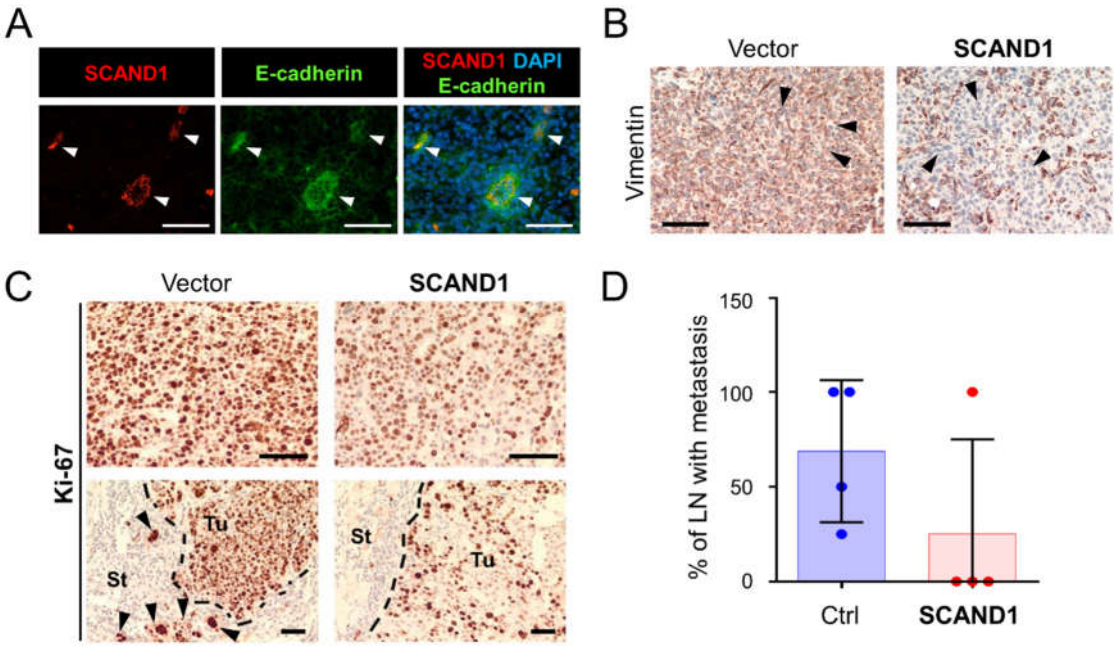

Figure 4. SCAND1 inhibits EMT, collective migration and lymph-node metastasis. SCAND1-overexpressed or the control vector-transfected DU-145 cells were subcutaneously transplanted into mice. Tumors were resected, and IHC was performed for SCAND1, E-cadherin, Vimentin and Ki-67. (A) Colocalization of SCAND1 and E-cadherin in the tumor overexpressed with SCAND1. Arrowheads indicate coexpression. Scale bars, 50 μm. (B) IHC for vimentin. Arrowheads indicate vimentin$^+$ cells in the left panel and vimentin$^-$ cells in the right panel. Scale bars, 50 μm. (C) IHC for Ki-67 in the center of tumors (upper panels) and tumor-stroma border areas (lower panels). St, stroma. Tu, tumor. Arrowheads indicate collectively migrating cells from the tumor into the stroma. Scale bars, 50 μm. (D) Column scatter plotting for the rate of lymph nodes with metastasis in each mouse. n=4 mice.

3.5. SCAND1 and MZF1 expression correlated with the prognosis of patients suffering from cancers

To clarify the prognostic values of MZF1 and SCAND1, we next investigated whether MZF1 and SCAND1 high or low expression correlated with survival rates of patients suffering from pancreatic, head and neck, kidney, and prostate cancers. High expression of MZF1 and SCAND1 correlated with better prognosis in pancreas DAC and head and neck SCC (Figure 5A, upper 4 panels; Table 2). On the other hand, high expression of MZF1 and SCAND1 correlated with poorer prognosis in kidney RCC (Figure 5A, third row; Table 2). Moreover, high expression of MZF1 correlated with poorer prognosis in prostate

 doi:10.20944/preprints202210.0475.v1

adenocarcinoma (Figure 5A, bottom). Meanwhile, Kaplan-Meyer graphs of SCAND1 high versus low expression cross each other and there was no correlation with the prognosis of prostate adenocarcinoma.

These data suggest that SCAND1-MZF1 high expression is a better prognosis marker for patients suffering from pancreatic cancer and head and neck cancer, whereas SCAND1-MZF1 high expression is a poorer prognosis marker for patients suffering from kidney cancer. MZF1 high expression is a poorer prognosis marker for patients suffering from prostate adenocarcinoma.

Table 2. Prognostic values of SCAND1 and MZF1 expression in cancer.

Cancer type	Log-rank P		Hazard ratio	
	SCAND1	**MZF1**	**SCAND1**	**MZF1**
Pancreas DAC	0.0041**	0.0009**	0.49	0.5
Head & Neck SCC, Stage III	0.024*	0.018*	0.40	0.26
Kidney RCC	9.9e-5***	1.7e-8***	1.79	2.38
Prostate Adenocarcinoma	0.15	0.002**	0.21	0.0062

*p<0.05, **p<0.05, ***p<0.0001.

Preprints (www.preprints.org) | NOT PEER-REVIEWED | Posted: 31 October 2022 doi:10.20944/preprints202210.0475.v1

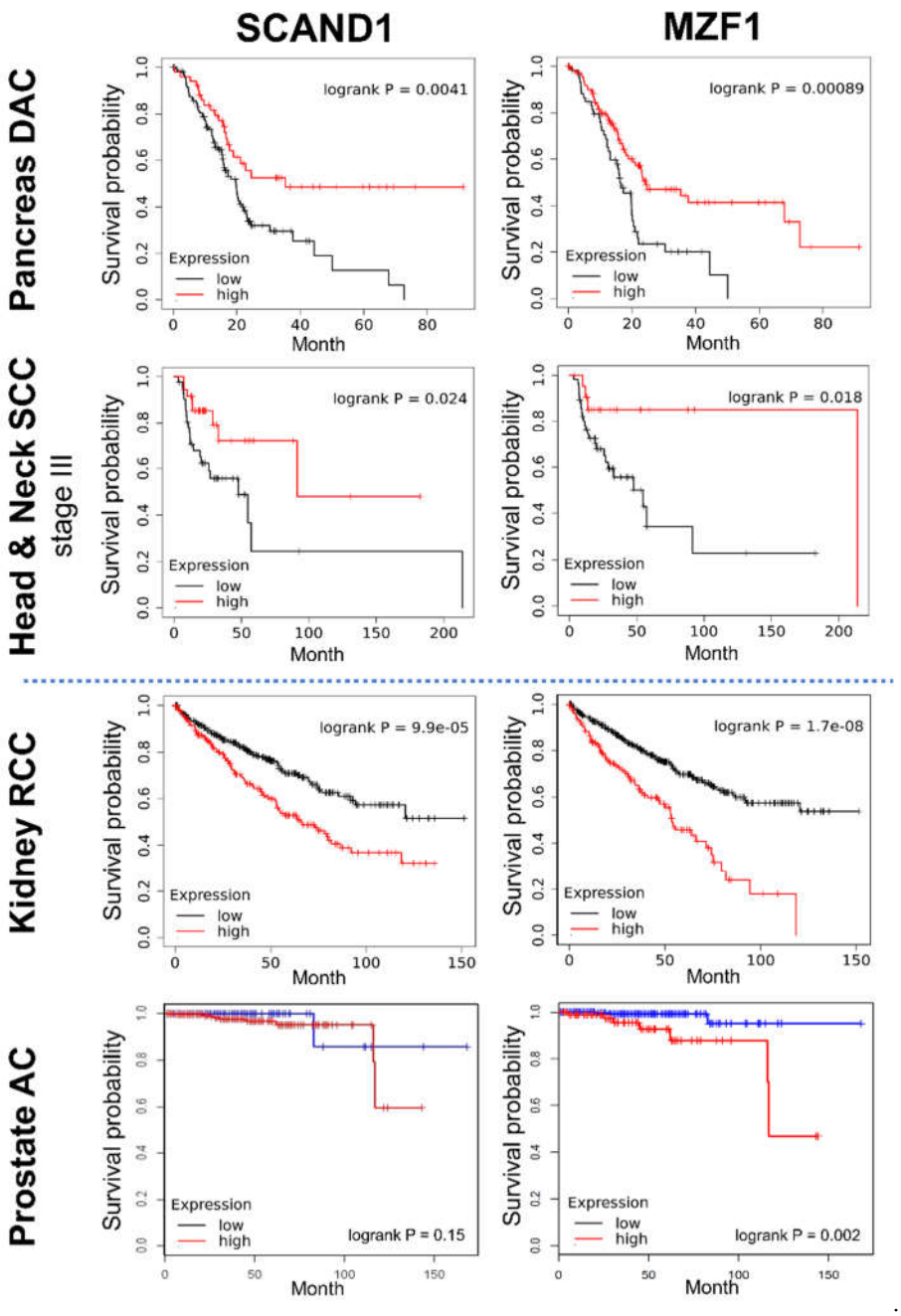

Figure 5. Prognostic values of SCAND1 and MZF1 expression in cancer patients. Kaplan-Meier plotting was performed to compare the prognosis of high- versus low-expression groups of SCAND1 and MZF1 in patients suffering from pancreas cancer, head and neck cancer, kidney cancer, and prostate cancer.

4. Discussion

In the present study, we show for the first time that SCAND1 reverses EMT, inhibits tumor cell proliferation and reduces the invasive capacities of prostate cancer cells (Figure 2). The rationale behind these properties is that SCAND1 can bind MZF1, a SCAN-ZF partner, binding to DNA and repress the transcription of pro-malignant target genes. We have shown direct evidence for MZF1-SCAND1 co-association on DNA and influence of the transcription of the CDC37 gene [28]. Evidence suggesting a role for these findings in prostate cancer is that SCAND1 and MZF1 are coordinately expressed in many cases of clinical prostate adenocarcinomas and are spacially co-localized in cancer cells. These findings suggest their oligomerization and co-regulation on target genes (Figure 1E, F).

Preprints (www.preprints.org) | NOT PEER-REVIEWED | Posted: 31 October 2022 doi:10.20944/preprints202210.0475.v1

Of note, overexpression of SCAND1 over endogenous MZF1 reverted partial EMT status of cells into a epithelia-like status, while combined SCAND1 and MZF1 expression negatively correlated with gene expression of EMT drivers, including ZEB1, ZEB2, TGFβ receptors and β-catenin (Figure 2 and 3). These data suggested that SCAND1-MZF1 complexes inhibit EMT by co-repressing ZEB1/2, TGFBRs and CTNNB1 (Figure 6). Moreover, overexpression of SCAND1 inhibited phosphorylation of ERK-1/2 and tumor cell proliferation, while SCAND1 and MZF1 expression negatively correlated with gene expression of MAP3K-1/2 (MEKK-1/2) (Figures 2 and 3). These data suggested that SCAND1-MZF1 complexes suppress tumor cell proliferation by co-repressing MEKK / MAP3K genes and quenching the MEK-ERK signaling pathway.

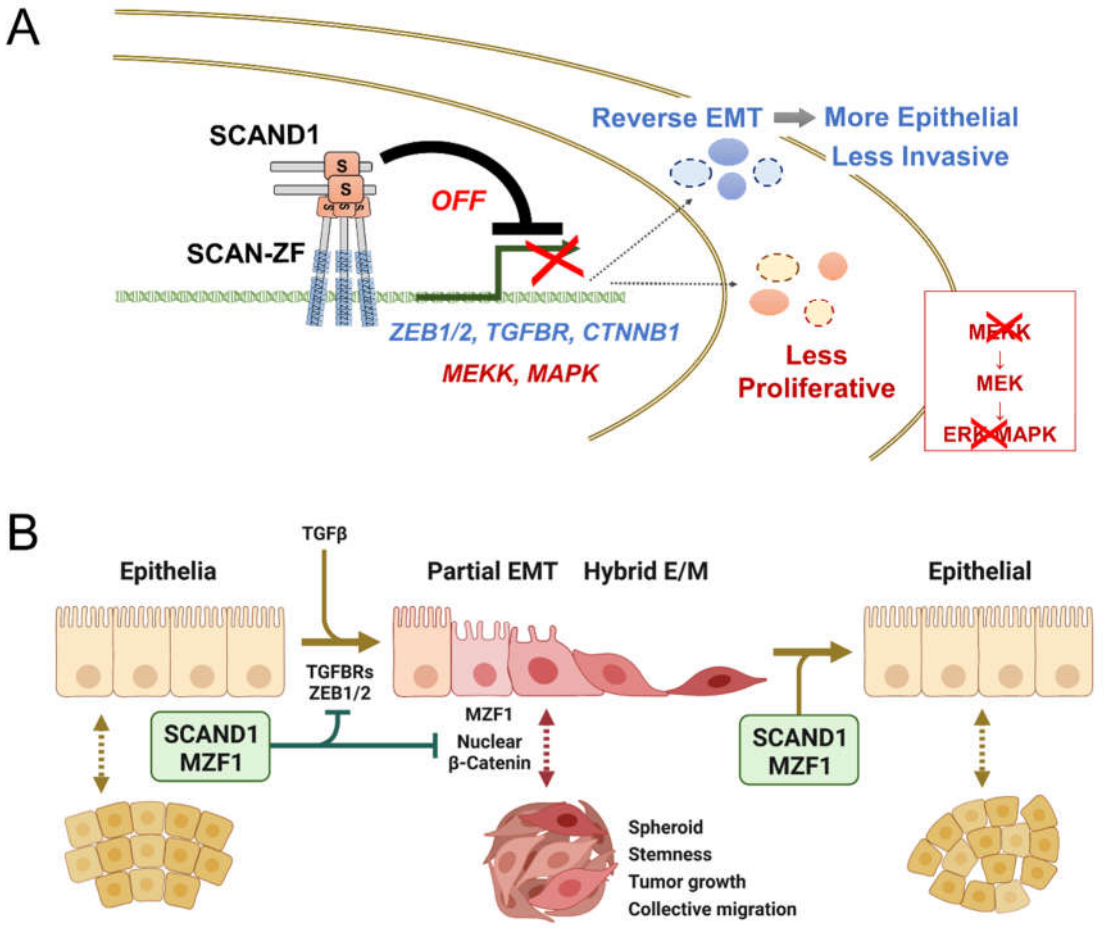

Figure 6. Graphical abstract. SCAND1-MZF1 can revert mesenchymal tumor cells to a more epithelial, less invasive status and inhibit their proliferation. (A) Transcriptional repression. The combination of SCAND1 and SCAN-ZF, such as MZF1, can repress EMT driver genes, including ZEB1/2, TGFBRs, CTNNB1 to reverse EMT for establishing more epithelial and less invasive phenotype. SCAND1-MZF1 also co-represses genes encoding mitogen-activated protein kinases, including MEKK and ERK-MAPK, to inhibit tumor cell proliferation. (B) Partial EMT (or hybrid E/M) is controlled by SCAND1-MZF1. SCAND1-MZF1 maintains epithelial status of cells, whereas the loss of SCAND1 initiate EMT. SCAND1-MZF1 co-expression can revert EMT to retrieve epithelial status. .

A therapeutic strategy to transduce mesenchymal tumor cells into epithelial cells by inducing SCAND1-MZF1 could potentially help cancer therapy. Epithelial tumor cells tend to be more sensitive to drugs, responsive to apoptosis signals, and susceptible to immune attack than mesenchymal tumor cells, whereas mesenchymal tumor cells are more chemoresistant [19]. However, a tumor epithelialization strategy could be context-dependent, as partial EMT induces tumor cell stemness, tumor initiation capacity, and adaptation to changes in the microenvironment and metabolism, which could generate

 doi:10.20944/preprints202210.0475.v1

resistant cancer reccurence that is difficult to treat [18]. Indeed, tumor cell spheroids are formed with epithelial adhesion by E-cadherin and EpCAM, while simultaneously expressing mesenchymal marker Vimentin, indicating that hybrid / partial EMT status may be essential for tumor and spheroid formation [13]. Moreover, spheroid formation involves enhanced stemness, chemoresistance, and malignant exosome release in cancer [13,49-52]. Our data indicate that elevated expression of SCAND1 and MZF1 can revert the hybrid EMT status of tumor cells to more epithelial status, although Vimentin and nuclear E-cadherin and β-catenin remained, suggesting that the cells were not fully epithelial.

Our study also suggests that the SCAND1-MZF1 complex is pleiotropic and can control several signaling pathways that activate EMT. These include TGFβ signal as well as Wnt-β-catenin pathway and MAPK signaling pathway, as suggested in Figures 2, 3 and Table 1. These findings are significant as TGFβ plays a central role in inducing EMT in several different tissue and tumor types [53-55]. This EMT signaling mechanism collaborates with several other signaling systems, including the MAPK (MEKK-MEK-ERK/MAPK and p38-MAPK) and PI3K-AKT-NF-κB pathways that also contribute to the expression of EMT programs [53]. Our data also suggest that SCAND1 and MZF1 could co-suppress WNT/β-catenin signal. Therefore, SCAND1-MZF1-based gene repression of CTNNB1 can minimize EMT-TF gene expression and thus reverse EMT. Our experiments also indicated that SCAND1-MZF1 can minimize the tumor microenvironmental EMT-inducing mitogenic factors, such as EGF, FGF, extracellular HSP90, and exosomes involved in activating EMT [10,56,57]. Therefore, SCAND1-MZF1-based gene repression of MAP3Ks and MAPKs can reduce mitogenic and EMT-inducing signals from EGFR and FGFR.

Our data suggest that SCAND1 and MZF1 might also be involved in regulating molecular chaperone expression and the cell stress response in cancer. We have shown that molecular chaperones HSP90 and CDC37 and HSP90-rich exosomes are crucial in promoting EMT in prostate cancer, tongue cancer, and normal epithelial cells [9,10,12]. The production of HSP90 / CD9-rich exosomes and the progression of EMT are regulated by heat shock factor 1 (HSF1) and its target gene CDC37 [9]. We also have shown that MZF1 activated the CDC37 gene, although SCAND1 repressed it in prostate cancer [28]. Therefore, SCAND1 and MZF1 could also be involved in cell stress response by crosstalking with oncogenic factor HSF1.

Finally, our data also touch upon potential prognostic importance of SCAND1 and MZF1 expression in evaluating several types of cancer, including prostate cancer. MZF1 and SCAND1 high expression correlated with better prognoses in patients suffering from pancreatic cancer and head and neck cancers (Figure 5), suggesting that elevated SCAND1-MZF1 co-expression could function by inhibiting EMT and invasive phenotypes promoting cancer. It was consistently reported that the downregulation of MZF1 is associated with gastric tumourigenesis, suggesting that MZF1 could be an early predictive and prognostic biomarker in gastric cancer patients [58]. On the other hand, SCAND1 and MZF1 high co-expression correlated with poor prognosis in patients suffering from kidney cancer. Hybrid EMT status can provide increased stemness, tumor initiation capacity, and the ability to adapt to environmental changes [18]. This status could affect the prognosis of cancer.

In conclusion, our current study suggests that the association of SCAND1 and MZF1 can revert the EMT phenotype and inhibit tumor cell proliferation by co-repressing the expression of MAP3K (MEKK), MAPK, and EMT driver genes in prostate cancer. SCAND1-MZF1 complexes can thus oppose tumor progression.

Author Contributions: T.E. conceived, conceptualized and designed the study. T.E. performed in-vitro experiments. E.C. and B.W. performed animal experiments and immunohistochemistry. T.E. analyzed clinical data. T.L.P constructed plasmids. T.E. and B.W. interpreted the data. T.E. wrote a draft of the manuscript. T.L.P., B.W. and S.K.C. revised and edited the manuscript.

Funding: T.E. was supported by JSPS Kakenhi grants 17K11642-TE, 20K09904-CS, 20H03888-HN, 20K20611-MT, 21H03119-TY, 21K08902-HY, 22H03511-HO, and 22F22409-MS/TE, Wesco Scientific Promotion Foundation, and Okayama University. B.W. was supported by NIH grants R21CA169904 and R01DK104714. S.K.C. was supported by NIH grants R01CA176326 and CA176326-05.

Institutional Review Board Statement: The animal study protocol was approved by the Institutional Ethics Commiitte of Beth Israel Deaconess Medical Center (protocol code 073-2017).

Data Availability Statement: TCGA PanCancer Atlas and coexpression data are availabe in cBioPortal (cbioportal.org/). Kaplan-Meyer datasets are available in KM plotter (kmplot.com) and GEPIA2 (gepia2.cancer-pku.cn).

Acknowledgments: We appreciate Benjamin Lang, Ayesha Murshid, Kuniaki Okamoto, Yuka Okusha, and Chiharu Sogawa for useful discussion, technical assistance, and lab management. Graphical abstract was partially generated using BioRender.

Conflicts of interest: The authors declare no conflict of interest.

References

1. Nieto, M.A. Epithelial-Mesenchymal Transitions in development and disease: old views and new perspectives. *Int J Dev Biol* **2009**, *53*, 1541-1547.
2. Nieto, M.A.; Huang, R.Y.; Jackson, R.A.; Thiery, J.P. Emt: 2016. *Cell* **2016**, *166*, 21-45.
3. Kalluri, R.; Weinberg, R.A. The basics of epithelial-mesenchymal transition. *J Clin Invest* **2009**, *119*, 1420-1428.
4. Thiery, J.P.; Acloque, H.; Huang, R.Y.; Nieto, M.A. Epithelial-mesenchymal transitions in development and disease. *Cell* **2009**, *139*, 871-890.
5. Yang, J.; Antin, P.; Berx, G.; Blanpain, C.; Brabletz, T.; Bronner, M.; Campbell, K.; Cano, A.; Casanova, J.; Christofori, G., *et al.* Guidelines and definitions for research on epithelial-mesenchymal transition. *Nat Rev Mol Cell Biol* **2020**, *21*, 341-352.
6. Dongre, A.; Weinberg, R.A. New insights into the mechanisms of epithelial–mesenchymal transition and implications for cancer. *Nat Rev Mol Cell Biol* **2019**, *20*, 69-84.
7. Krebs, A.M.; Mitschke, J.; Lasierra Losada, M.; Schmalhofer, O.; Boerries, M.; Busch, H.; Boettcher, M.; Mougiakakos, D.; Reichardt, W.; Bronsert, P., *et al.* The EMT-activator Zeb1 is a key factor for cell plasticity and promotes metastasis in pancreatic cancer. *Nat Cell Biol* **2017**, *19*, 518-529.
8. Ye, X.; Tam, W.L.; Shibue, T.; Kaygusuz, Y.; Reinhardt, F.; Ng Eaton, E.; Weinberg, R.A. Distinct EMT programs control normal mammary stem cells and tumour-initiating cells. *Nature* **2015**, *525*, 256-260.
9. Eguchi, T.; Sogawa, C.; Ono, K.; Matsumoto, M.; Tran, M.T.; Okusha, Y.; Lang, B.J.; Okamoto, K.; Calderwood, S.K. Cell Stress Induced Stressome Release Including Damaged Membrane Vesicles and Extracellular HSP90 by Prostate Cancer Cells. *Cells* **2020**, *9*, 1-24.
10. Fujiwara, T.; Eguchi, T.; Sogawa, C.; Ono, K.; Murakami, J.; Ibaragi, S.; Asaumi, J.; Calderwood, S.K.; Okamoto, K.; Kozaki, K. Carcinogenic epithelial-mesenchymal transition initiated by oral cancer exosomes is inhibited by anti-EGFR antibody cetuximab. *Oral Oncol* **2018**, *86*, 251-257.
11. Rhim, A.D.; Mirek, E.T.; Aiello, N.M.; Maitra, A.; Bailey, J.M.; McAllister, F.; Reichert, M.; Beatty, G.L.; Rustgi, A.K.; Vonderheide, R.H., *et al.* EMT and dissemination precede pancreatic tumor formation. *Cell* **2012**, *148*, 349-361.
12. Ono, K.; Sogawa, C.; Kawai, H.; Tran, M.T.; Taha, E.A.; Lu, Y.; Oo, M.W.; Okusha, Y.; Okamura, H.; Ibaragi, S., *et al.* Triple knockdown of CDC37, HSP90-alpha and HSP90-beta diminishes extracellular vesicles-driven malignancy events and macrophage M2 polarization in oral cancer. *J Extracell Vesicles* **2020**, *9*, 1-21.
13. Eguchi, T.; Sogawa, C.; Okusha, Y.; Uchibe, K.; Iinuma, R.; Ono, K.; Nakano, K.; Murakami, J.; Itoh, M.; Arai, K., *et al.* Organoids with Cancer Stem Cell-like Properties Secrete Exosomes and HSP90 in a 3D NanoEnvironment. *PLoS One* **2018**, *13*, e0191109.
14. Pastushenko, I.; Blanpain, C. EMT Transition States during Tumor Progression and Metastasis. *Trends Cell Biol* **2019**, *29*, 212-226.
15. Ruscetti, M.; Quach, B.; Dadashian, E.L.; Mulholland, D.J.; Wu, H. Tracking and Functional Characterization of Epithelial-Mesenchymal Transition and Mesenchymal Tumor Cells during Prostate Cancer Metastasis. *Cancer Res* **2015**, *75*, 2749-2759.
16. Pastushenko, I.; Mauri, F.; Song, Y.; de Cock, F.; Meeusen, B.; Swedlund, B.; Impens, F.; Van Haver, D.; Opitz, M.; Thery, M., *et al.* Fat1 deletion promotes hybrid EMT state, tumour stemness and metastasis. *Nature* **2021**, *589*, 448-455.
17. Pastushenko, I.; Brisebarre, A.; Sifrim, A.; Fioramonti, M.; Revenco, T.; Boumahdi, S.; Van Keymeulen, A.; Brown, D.; Moers, V.; Lemaire, S., *et al.* Identification of the tumour transition states occurring during EMT. *Nature* **2018**, *556*, 463-468.
18. Brabletz, S.; Schuhwerk, H.; Brabletz, T.; Stemmler, M.P. Dynamic EMT: a multi-tool for tumor progression. *EMBO J* **2021**, *40*, e108647.
19. Jiang, Y.; Zhan, H. Communication between EMT and PD-L1 signaling: New insights into tumor immune evasion. *Cancer Lett* **2020**, *468*, 72-81.
20. Tadepally, H.D.; Burger, G.; Aubry, M. Evolution of C2H2-zinc finger genes and subfamilies in mammals: species-specific duplication and loss of clusters, genes and effector domains. *BMC Evol Biol* **2008**, *8*, 176.
21. Edelstein, L.C.; Collins, T. The SCAN domain family of zinc finger transcription factors. *Gene* **2005**, *359*, 1-17.

 doi:10.20944/preprints202210.0475.v1

22. Sander, T.L.; Stringer, K.F.; Maki, J.L.; Szauter, P.; Stone, J.R.; Collins, T. The SCAN domain defines a large family of zinc finger transcription factors. *Gene* **2003**, *310*, 29-38.
23. Schumacher, C.; Wang, H.; Honer, C.; Ding, W.; Koehn, J.; Lawrence, Q.; Coulis, C.M.; Wang, L.L.; Ballinger, D.; Bowen, B.R., *et al.* The SCAN domain mediates selective oligomerization. *J Biol Chem* **2000**, *275*, 17173-17179.
24. Williams, A.J.; Blacklow, S.C.; Collins, T. The zinc finger-associated SCAN box is a conserved oligomerization domain. *Mol Cell Biol* **1999**, *19*, 8526-8535.
25. Eguchi, T.; Prince, T.; Wegiel, B.; Calderwood, S.K. Role and Regulation of Myeloid Zinc Finger Protein 1 in Cancer. *J Cell Biochem* **2015**, *116*, 2146-2154.
26. Sander, T.L.; Haas, A.L.; Peterson, M.J.; Morris, J.F. Identification of a novel SCAN box-related protein that interacts with MZF1B. The leucine-rich SCAN box mediates hetero- and homoprotein associations. *J Biol Chem* **2000**, *275*, 12857-12867.
27. Perrotti, D.; Melotti, P.; Skorski, T.; Casella, I.; Peschle, C.; Calabretta, B. Overexpression of the zinc finger protein MZF1 inhibits hematopoietic development from embryonic stem cells: correlation with negative regulation of CD34 and c-myb promoter activity. *Mol Cell Biol* **1995**, *15*, 6075-6087.
28. Eguchi, T.; Prince, T.L.; Tran, M.T.; Sogawa, C.; Lang, B.J.; Calderwood, S.K. MZF1 and SCAND1 Reciprocally Regulate CDC37 Gene Expression in Prostate Cancer. *Cancers (Basel)* **2019**, *11*, 1-15.
29. Zheng, L.; Jiao, W.; Mei, H.; Song, H.; Li, D.; Xiang, X.; Chen, Y.; Yang, F.; Li, H.; Huang, K., *et al.* miRNA-337-3p inhibits gastric cancer progression through repressing myeloid zinc finger 1-facilitated expression of matrix metalloproteinase 14. *Oncotarget* **2016**, *7*, 40314-40328.
30. Ko, H.; Kim, S.; Yang, K.; Kim, K. Phosphorylation-dependent stabilization of MZF1 upregulates N-cadherin expression during protein kinase CK2-mediated epithelial-mesenchymal transition. *Oncogenesis* **2018**, *7*, 27.
31. Luan, H.; Mohapatra, B.; Bielecki, T.A.; Mushtaq, I.; Mirza, S.; Jennings, T.A.; Clubb, R.J.; An, W.; Ahmed, D.; El-Ansari, R., *et al.* Loss of the Nuclear Pool of Ubiquitin Ligase CHIP/STUB1 in Breast Cancer Unleashes the MZF1-Cathepsin Pro-oncogenic Program. *Cancer Res* **2018**, *78*, 2524-2535.
32. Verma, N.K.; Gadi, A.; Maurizi, G.; Roy, U.B.; Mansukhani, A.; Basilico, C. Myeloid Zinc Finger 1 and GA Binding Protein Co-Operate with Sox2 in Regulating the Expression of Yes-Associated Protein 1 in Cancer Cells. *Stem Cells* **2017**, *35*, 2340-2350.
33. Wu, L.; Han, L.; Zhou, C.; Wei, W.; Chen, X.; Yi, H.; Wu, X.; Bai, X.; Guo, S.; Yu, Y., *et al.* TGF-beta1-induced CK17 enhances cancer stem cell-like properties rather than EMT in promoting cervical cancer metastasis via the ERK1/2-MZF1 signaling pathway. *FEBS J* **2017**, *284*, 3000-3017.
34. Tsai, S.J.; Hwang, J.M.; Hsieh, S.C.; Ying, T.H.; Hsieh, Y.H. Overexpression of myeloid zinc finger 1 suppresses matrix metalloproteinase-2 expression and reduces invasiveness of SiHa human cervical cancer cells. *Biochem Biophys Res Commun* **2012**, *425*, 462-467.
35. Wu, D.; Tan, H.; Su, W.; Cheng, D.; Wang, G.; Wang, J.; Ma, D.A.; Dong, G.M.; Sun, P. MZF1 mediates oncogene-induced senescence by promoting the transcription of p16(INK4A). *Oncogene* **2022**, *41*, 414-426.
36. Weber, C.E.; Kothari, A.N.; Wai, P.Y.; Li, N.Y.; Driver, J.; Zapf, M.A.; Franzen, C.A.; Gupta, G.N.; Osipo, C.; Zlobin, A., *et al.* Osteopontin mediates an MZF1-TGF-beta1-dependent transformation of mesenchymal stem cells into cancer-associated fibroblasts in breast cancer. *Oncogene* **2015**, *34*, 4821-4833.
37. Krüger, M.; Metzger, C.; Al-Nawas, B.; Kämmerer, P.W.; Brieger, J. Cigarette smoke modulates binding of the transcription factor MZF1 to the VEGF promoter and regulates VEGF expression in dependence of genetic variation SNP 405. *J Oral Pathol Med* **2020**, *49*, 780-786.
38. Noll, L.; Peterson, F.C.; Hayes, P.L.; Volkman, B.F.; Sander, T. Heterodimer formation of the myeloid zinc finger 1 SCAN domain and association with promyelocytic leukemia nuclear bodies. *Leuk Res* **2008**, *32*, 1582-1592.
39. Eguchi, T.; Watanabe, K.; Hara, E.S.; Ono, M.; Kuboki, T.; Calderwood, S.K. OstemiR: a novel panel of microRNA biomarkers in osteoblastic and osteocytic differentiation from mesencymal stem cells. *PLoS One* **2013**, *8*, e58796.
40. Eguchi, T.; Kubota, S.; Kawata, K.; Mukudai, Y.; Uehara, J.; Ohgawara, T.; Ibaragi, S.; Sasaki, A.; Kuboki, T.; Takigawa, M. Novel transcription-factor-like function of human matrix metalloproteinase 3 regulating the CTGF/CCN2 gene. *Mol Cell Biol* **2008**, *28*, 2391-2413.
41. Okusha, Y.; Eguchi, T.; Tran, M.T.; Sogawa, C.; Yoshida, K.; Itagaki, M.; Taha, E.A.; Ono, K.; Aoyama, E.; Okamura, H., *et al.* Extracellular Vesicles Enriched with Moonlighting Metalloproteinase Are Highly Transmissive, Pro-Tumorigenic, and Trans-Activates Cellular Communication Network Factor (CCN2/CTGF): CRISPR against Cancer. *Cancers (Basel)* **2020**, *12*.
42. Li, C.; Tang, Z.; Zhang, W.; Ye, Z.; Liu, F. GEPIA2021: integrating multiple deconvolution-based analysis into GEPIA. *Nucleic Acids Res* **2021**, *49*, W242-w246.
43. Lánczky, A.; Győrffy, B. Web-Based Survival Analysis Tool Tailored for Medical Research (KMplot): Development and Implementation. *J Med Internet Res* **2021**, *23*, e27633.
44. Jongsma, J.; Oomen, M.H.; Noordzij, M.A.; Romijn, J.C.; van Der Kwast, T.H.; Schroder, F.H.; van Steenbrugge, G.J. Androgen-independent growth is induced by neuropeptides in human prostate cancer cell lines. *Prostate* **2000**, *42*, 34-44.
45. Li, C.F.; Chen, J.Y.; Ho, Y.H.; Hsu, W.H.; Wu, L.C.; Lan, H.Y.; Hsu, D.S.; Tai, S.K.; Chang, Y.C.; Yang, M.H. Snail-induced claudin-11 prompts collective migration for tumour progression. *Nat Cell Biol* **2019**, *21*, 251-262.
46. Chen, G.; Shukeir, N.; Potti, A.; Sircar, K.; Aprikian, A.; Goltzman, D.; Rabbani, S.A. Up-regulation of Wnt-1 and beta-catenin production in patients with advanced metastatic prostate carcinoma: potential pathogenetic and prognostic implications. *Cancer* **2004**, *101*, 1345-1356.

47. Rau, T.T.; Bettschen, E.; Buchi, C.; Christe, L.; Rohner, A.; Muller, M.D.; Carlson, J.W.; Imboden, S.; Zlobec, I. Prognostic impact of tumor budding in endometrial carcinoma within distinct molecular subgroups. *Mod Pathol* **2021**, *34*, 222-232.
48. Mitrovic, B.; Schaeffer, D.F.; Riddell, R.H.; Kirsch, R. Tumor budding in colorectal carcinoma: time to take notice. *Mod Pathol* **2012**, *25*, 1315-1325.
49. Arai, K.; Eguchi, T.; Rahman, M.M.; Sakamoto, R.; Masuda, N.; Nakatsura, T.; Calderwood, S.K.; Kozaki, K.; Itoh, M. A Novel High-Throughput 3D Screening System for EMT Inhibitors: A Pilot Screening Discovered the EMT Inhibitory Activity of CDK2 Inhibitor SU9516. *PLoS One* **2016**, *11*, e0162394.
50. Sogawa, C.; Eguchi, T.; Namba, Y.; Okusha, Y.; Aoyama, E.; Ohyama, K.; Okamoto, K. Gel-Free 3D Tumoroids with Stem Cell Properties Modeling Drug Resistance to Cisplatin and Imatinib in Metastatic Colorectal Cancer. *Cells* **2021**, *10*.
51. Taha, E.A.; Sogawa, C.; Okusha, Y.; Kawai, H.; Oo, M.W.; Elseoudi, A.; Lu, Y.; Nagatsuka, H.; Kubota, S.; Satoh, A., *et al.* Knockout of MMP3 Weakens Solid Tumor Organoids and Cancer Extracellular Vesicles. *Cancers (Basel)* **2020**, *12*.
52. Namba, Y.; Sogawa, C.; Okusha, Y.; Kawai, H.; Itagaki, M.; Ono, K.; Murakami, J.; Aoyama, E.; Ohyama, K.; Asaumi, J., *et al.* Depletion of Lipid Efflux Pump ABCG1 Triggers the Intracellular Accumulation of Extracellular Vesicles and Reduces Aggregation and Tumorigenesis of Metastatic Cancer Cells. *Front Oncol* **2018**, *8*, 1-16.
53. Lamouille, S.; Xu, J.; Derynck, R. Molecular mechanisms of epithelial-mesenchymal transition. *Nat Rev Mol Cell Biol* **2014**, *15*, 178-196.
54. Xu, J.; Lamouille, S.; Derynck, R. TGF-beta-induced epithelial to mesenchymal transition. *Cell Res* **2009**, *19*, 156-172.
55. Bierie, B.; Moses, H.L. TGF-beta and cancer. *Cytokine Growth Factor Rev* **2006**, *17*, 29-40.
56. Fujiwara, T.; Eguchi, T.; Sogawa, C.; Ono, K.; Murakami, J.; Ibaragi, S.; Asaumi, J.; Okamoto, K.; Calderwood, S.K.; Kozaki, K. Anti-EGFR antibody cetuximab is secreted by oral squamous cell carcinoma and alters EGF-driven mesenchymal transition. *Biochem Biophys Res Commun* **2018**, *503*, 1267-1272.
57. Wang, Q.; Liao, C.; Tan, Z.; Li, X.; Guan, X.; Li, H.; Tian, Z.; Liu, J.; An, J. FUT6 inhibits the proliferation, migration, invasion, and EGF-induced EMT of head and neck squamous cell carcinoma (HNSCC) by regulating EGFR/ERK/STAT signaling pathway. *Cancer Gene Ther* **2022**.
58. Li, G.Q.; He, Q.; Yang, L.; Wang, S.B.; Yu, D.D.; He, Y.Q.; Hu, J.; Pan, Y.M.; Wu, Y. Clinical Significance of Myeloid Zinc Finger 1 Expression in the Progression of Gastric Tumourigenesis. *Cell Physiol Biochem* **2017**, *44*, 1242-1250.